Electroluminescence of erbium-doped silicon

J. Palm, F. Gan, B. Zheng, J. Michel, and L. C. Kimerling
Massachusetts Institute of Technology, Department of Materials Science and Engineering, 77 Massachusetts Avenue, Cambridge, Massachusetts 02139
(Received 1 February 1996; revised manuscript received 1 May 1996)

Recombination processes in rare-earth metals in semiconductors are a special case due to the localized nature of *f* electrons. Our work explores in detail the radiative and nonradiative mechanisms of energy transfer for erbium in silicon by investigating the temperature dependence of the intensity and the decay time of the photoluminescence of Er-related centers in Si. We show that nonradiative energy back transfer from the excited Er $4f$ shell causes luminescence quenching below 200 K. We study electroluminescence decay by applying different bias conditions during the decay. In a two-beam experiment the photoluminescence decay is monitored for different background-excitation laser powers. Changes in the decay time are strong evidence of the impurity Auger effect as an efficient luminescence-quenching mechanism for Er in Si. A fast initial luminescence decay component at high pumping powers is related to quenching by excess carriers. The power dependence, the decay-time components, and the two-beam experiment are simulated by a set of rate equations which involve the formation of excitons, a decrease of the pumping efficiency by exciton Auger recombination, and a decrease of radiative efficiency by the impurity Auger effect with free electrons. As a nonradiative deexcitation path competing with spontaneous emission, the impurity Auger effect decreases the excited-state lifetime of Er in Si, and dominates the thermal quenching of luminescence in the temperature range from 4 to 100 K. We find that the decrease of emission intensity above 100 K is caused by an unidentified second back-transfer process. [S0163-1829(96)07040-3]

I. INTRODUCTION

A. General

Since the first report in 1983,[1] both scientific and technology-motivated research has increasingly focused on the luminescence of Er in Si. By building the first Si-based light-emitting diode (LED), which operates at room temperature at $\lambda=1.54$ μm, we found that Er doping of Si is a viable approach toward a Si microphotonic technology.[2,3] Our objective is to establish an integrated-circuit-compatible process technology for integration of optical interconnection with Si electronics. Current research in the field addresses material properties of the Si:Er system,[4–6] optical activation and luminescence enhancement by codoping of impurities,[7–11] and the physics of the Er luminescence.[12–14]

In this paper[15] we analyze in detail the excitation and deexcitation processes of the Si:Er center. The sharp line luminescence at $\lambda=1.54$ μm arises from the $^4I_{13/2}\Rightarrow{}^4I_{15/2}$ transition from the excited, inner $4f$ (Ref. 11) shell of the Er^{3+} configuration. In contrast to other luminescent processes in semiconductors, rare-earth luminescence arises from spin-state transitions; therefore it does not directly involve changes of charge state or the occupancy of bands, or band-gap states. The luminescence of Er in Si is always electroluminescence (EL), in that excitation involves the generation of electron-hole pairs followed by a nonradiative energy transfer of the recombination energy to the Er inner $4f$ shell.[16] A theoretical evaluation of the excitation process suggests that an intracenter Auger process[17] provides the energy transfer to the $4f$ shell by electric dipole and exchange interactions. The efficiency of this process is greatly enhanced if a state in the band gap associated with the Er center allows a localization of energy in the form of bound excitons. In Sec. IV D we show that at low temperatures the dominant processes after excess carrier generation are the formation of excitons and their subsequent recombination by Auger processes. Recombination by nonradiative energy transfer to free carriers competes with the Si:Er excitation process [Figs. 1(a) and 1(b)]. We show in Sec. III that the electroluminescence of Er in Si is far more efficient than direct optical pumping of Er-doped fibers for optical amplifiers.

B. Energy flow for recombination at rare-earth centers in semiconductors

It is important to understand the kinetic regimes of energy flow for recombination at rare-earth centers in semiconductors. The rate-limiting step for electron-hole recombination is the dissipation of the energy difference between the initial and final states. Figure 1(a) depicts a serial sequence of energy transfer comprised of four regimes. In a serial sequence of events, the slowest process dominates. In regimes I, III, and IV, parallel processes compete for the energy flow. For parallel processes the fastest mechanism will dominate. All processes preceding or competing with the Auger Er excitation will determine the emission intensity without affecting the luminescence decay time. In regime IV, both the decay time and the emission intensity are controlled by the fastest of the two processes. For slow nonradiative back-transfer processes, the spontaneous emission lifetime of the excited state of the rare-earth (RE) center is observed. For fast back transfer, the rate of nonradiative energy flow is observed, and the radiative emission is reduced.

As an internal, discrete-to-discrete $4f$ state transition, the Er luminescence energy is independent of band gap and,

 © 1996 The American Physical Society

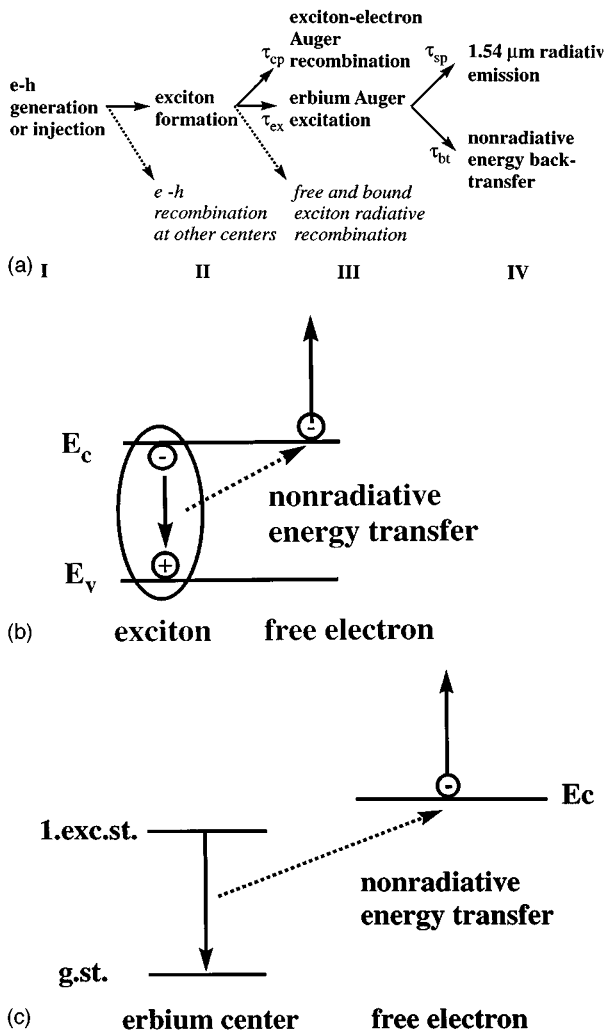

FIG. 1. (a) Excitation and deexcitation processes of Er in Si. All processes in bold letters are comprised in a model which is presented in Sec. IV C to describe the low-temperature Er luminescence phenomena. (b) Exciton-electron Auger recombination process. (c) Energy back transfer from the excited Er $4f$ shell by an impurity Auger process with free carriers.

hence, does not change with temperature. The emission intensity, however, can strongly decrease by as much as three orders of magnitude as the temperature increases from 4 to 300 K. The following are three different possible causes for the observed thermal quenching.

(1) The total number of optically active, excitable Er centers decreases, for example, by a temperature-controlled structural transition to a nonluminescent configuration.

(2) The pumping efficiency decreases by processes occurring between electron-hole pair generation and the Er excitation. These are the processes in regimes I–III of Fig. 1(a), such as competing recombination processes, e.g., via deep traps and Auger processes [Fig. 1(b)], or the decrease of the excitation efficiency by thermalization of carriers from an Er-related state in the band gap.

(3) The radiative efficiency decreases by a nonradiative energy back transfer from the excited Er $4f$ shell [regime IV of Fig. 1(a)]. Possible energy back-transfer mechanisms are multiphonon emission processes or impurity Auger processes involving the energy transfer by electric dipole or exchange interaction between the $4f$ electrons and free or bound carriers [Fig. 1(c)].

This work demonstrates that energy back-transfer processes are responsible for the thermal quenching of the Er luminescence in Si below 200 K. The direct evidence of back-transfer processes is the correlation of photoluminescence decay time and intensity. A decrease of Si:Er decay time by a shortening of the spontaneous emission time should lead to an increase of luminescence intensity. We observe a decrease of the lifetime with a concurrent loss of emission intensity. This correlation argues strongly for a fast, competing nonradiative process of energy back transfer from the excited Er center to the crystal host.

We show that the impurity Auger effect decreases the excited-state lifetime of Er in Si, and controls the thermal quenching in the temperature range from 4 to 100 K. Measurements of the dependence of photoluminescence intensity vs excitation power show that at 4 K the internal quantum efficiency decreases by three orders of magnitude with increasing pump power. We demonstrate that impurity Auger recombination and exciton-electron Auger recombination can reduce both the pumping and the radiative efficiency of Si:Er [Figs. 1(a)–1(c)].

II. EXPERIMENT

Boron-doped Czochralski-grown Si wafers were implanted with Er and O, resulting in peak concentrations of 5×10^{17} and 3×10^{18} cm^{-3}. We used two different implantation energies 4.5 MeV and 400 keV for Er, which correspond to peak depths of 1.4 μm (deep) and 0.130 μm (shallow), respectively. The oxygen implant energies were chosen accordingly to match the Er profiles. For this paper we consider four types of samples: sample *A* (deep implant) and *B* (shallow implant) were subsequently annealed at 900 °C for 30 min in an argon ambient. Mesa LED structures were fabricated with an As *n* emitter by implantation prior to the Er/O implantation. For sample *C* (deep implant) the emitter implant was annealed at 1000 °C for 2 h. After Er/O implantation the Si-Er centers were activated by the same 900 °C/30-min anneal. For sample *D* the (shallow) As/Er/O LED implants were annealed together at 800 °C for 30 min. After annealing, open Al front contacts were formed.[2] For photoluminescence (PL) spectra a mechanically chopped $\lambda=488$-nm Ar-ion laser beam provided the excitation. For EL spectra the devices were forward biased with a pulsed voltage generator. A liquid-nitrogen (LN)-cooled Ge detector, a grating spectrometer, and a lock-in amplifier were used for signal detection. For the decay measurements the latter components were replaced by a 1.54-μm/40-nm bandpass filter, a LN-cooled $In_xGa_{1-x}P$ detector, a current amplifier, and a digital oscilloscope. The measurement system response time was 20 μs.

III. EFFICIENCY OF ELECTROLUMINESCENCE OF Er IN Si

Er doping is employed in glass hosts for commercial lasers and optical amplifiers. These devices operate by optical pumping at $\lambda=960$ nm. In contrast, the pumping of Si:Er is

always mediated by electron-hole recombination. The efficiencies of these two different excitation mechanisms may be compared by relating the incident flux (photons or electrons per second) to the emitted photon flux. Optical excitation is commonly characterized by the photon capture cross section σ_0, as defined by the equation

$$\Phi_{\text{out}} = \sigma_0 \Phi_{\text{in}} N_{\text{er}}, \tag{1}$$

where N_{Er} is the density of Er centers integrated over the depth. For the case of Er incorporation by ion implantation, this value corresponds to the implanted Er dose. Φ_{in} and Φ_{out} are the incident and emitted photon fluxes. To calculate the ''effective photon capture cross section'' for Si:Er from our photoluminescence experiments at 4 K, we intentionally abstract from all processes between photon absorption by the Si host and light emission from the Si:Er center. The lowest and highest laser powers which we applied are 10 μW and 1.6 W. Losses due to cryostat windows and Si surface reflection reduce the absorbed power by about 70%. At the argon-ion laser wavelength of $\lambda = 488$ nm the coupled incident photon fluxes (Φ_{in}) are of 7.4×10^{12} and 1.2×10^{18} s^{-1}, respectively. Taking into account the extraction losses due to total internal reflection and light collection due to the experimental geometry, we obtain, at 4 K, typical total output powers of 0.15 and 10 μW which correspond to emitted photon fluxes (Φ_{out}) of 1.2×10^{12} and 7.8×10^{13} s^{-1} at $\lambda = 1.54$ μm for the two different injection levels. With the Er dose $N_{\text{Er}} = 3\times10^{13}$ cm^{-2}, Eq. (1) yields values for the ''effective photon capture cross section'' of $\sigma_0 = 5.2\times10^{-15}$ and $\sigma_0 = 2.2\times10^{-18}$ cm^2 for the low- and high-power excitation, respectively.

Comparing to the value of $\sigma_0 = 2\times10^{-21}$ cm^2 for Er in glass hosts,[18] we can conclude that the electrical excitation of the Er $4f$ shell luminescence is 3–6 orders of magnitude more efficient in Si than optical excitation in glass hosts. The internal quantum efficiency η_i, however, is low compared to III–V band-edge luminescence: for these samples it ranges from 5% to 0.002% at the lowest and highest powers, respectively. In Sec. IV we show that the decrease of η_i and σ_0 with excitation power is due to Auger processes that decrease both the pumping and radiative efficiency.

IV. RESULTS

A. Dependence of emission intensity on temperature and pumping power

Figure 2 shows the dependence of PL intensity on temperature in a semilog plot for two different pumping powers. There are two distinct regimes indicating two different mechanisms which are responsible for the thermal quenching of the emission intensity. A double-exponential fit (solid line), by the equation

$$I(T) = I_0 \left\{ 1 + c_1 \exp\left(-\frac{E_1}{k\cdot T} \right) + c_2 \exp\left(-\frac{E_2}{k\cdot T} \right) \right\}, \tag{2}$$

gives activation energies of $E_1 = 10$ meV and $E_2 = 160$ meV for both pumping laser powers. The fitting parameters c_1 and c_2 can be understood as coupling coefficients for two activated processes. They depend, however, on excitation power because the quenching rate $I(T)/I_0$ decreases with increasing excitation power. In Secs. IV D and IV E we present evidence that the two apparent processes are backtransfer processes.

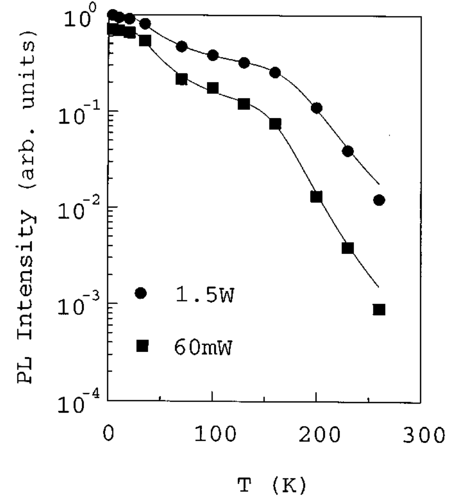

FIG. 2. PL intensity vs temperature for two different excitation laser powers (sample C).

Figure 3 presents the dependence of PL intensity on laser power for different temperatures in a log-log plot. In this plot the slope of the curves increases with increasing temperature. The log-log plot reveals that particularly at the two lower temperatures the dependence cannot be described by a simple power law. The calculation of internal quantum efficiency in Sec. III yielded a decrease of three orders of magnitude over the measured range of five decades of incident laser powers (10 μW to 1.6 W). We show below that the decrease of the total efficiency is caused by Auger processes affecting both the pumping efficiency η_{pump} and the radiative efficiency η_{rad}. Internal quantum efficiency can be described as the product of the pumping efficiency η_{pump} and the radiative efficiency η_{rad}:

$$\eta = \eta_{\text{pump}} \eta_{\text{rad}} = \frac{1}{\left(1 + \frac{\tau_{\text{ex}}}{\tau_{\text{cp}}}\right)} \frac{1}{\left(1 + \frac{\tau_{\text{sp}}}{\tau_{\text{bt}}}\right)}. \tag{3}$$

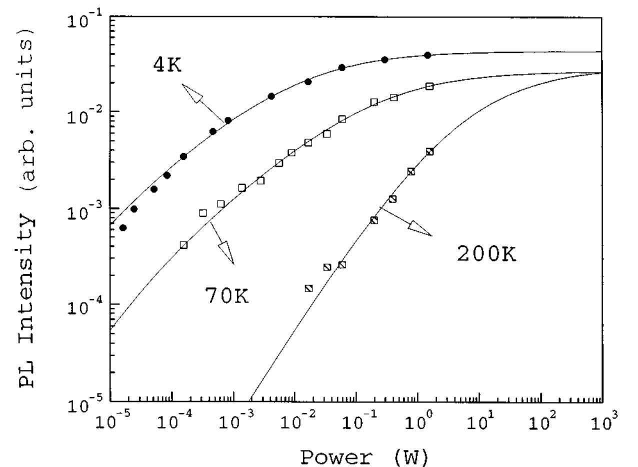

FIG. 3. PL intensity vs. excitation power for three different temperatures (sample C).

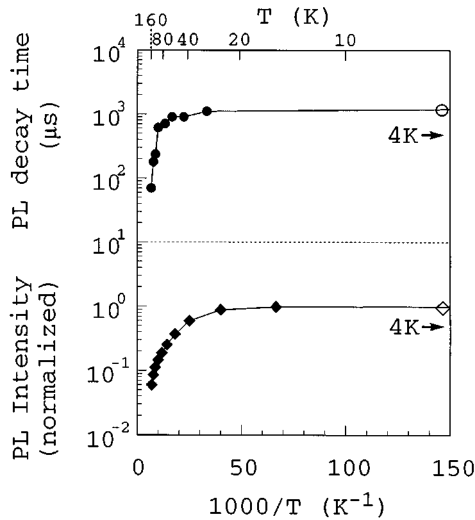

FIG. 4. Temperature dependence of $1/e$ decay time (top) and intensity (bottom) measured at low power (PL, 60 mW, sample A).

The first factor (η_{pump}) reflects the temporal branching in regime III [Fig. 1(a)] by processes (τ_{cp}) competing with the excitation (τ_{ex}). The second factor (η_{rad}) represents back-transfer processes (τ_{bt}) competing in regime IV with spontaneous emission time (τ_{sp}).

In the case of Auger processes with excess carriers, we expect that the probabilities of competitive (τ_{cp}^{-1}) and back-transfer (τ_{bt}^{-1}) processes are proportional to the free-carrier density. Due to the indirect band gap of silicon the excess carrier density is controlled by the bimolecular formation of excitons at low temperatures, and is therefore proportional to the square root of generation rate, i.e., the pumping power. In Sec. IV C we will confirm the square-root dependence by a two-beam PL experiment. We find, indeed, that all three curves can be fit by the following function of pumping power p, which is similar to Eq. (3):

$$I(p)=\frac{\eta}{h\cdot\nu}\,p=\frac{c_3 p}{(c_4+\sqrt{p})(c_5+\sqrt{p})}, \tag{4}$$

where c_3, c_4, and c_5 are fitting parameters. At 4 K the output intensity apparently saturates at high powers (slope equals to zero). This maximum intensity value corresponds to the fitting parameter c_3. All curves were fitted independently. The parameter c_3 varies only by about 40% for the three temperatures. The parameters c_4 and c_5 increase with increasing temperature: at 4 K, $c_4=0.002$, $c_5=0.125$; at 70 K, $c_4=0.006$, $c_5=0.5$; and at 200 K, $c_4=3$, $c_5=3$. Since parameter c_3 remains approximately constant, this fitting function predicts saturation at about the same intensity at high pump powers independent of measurement temperature, as evident in Fig. 3. The fitting function [Eq. (4)] is the analytical steady-state solution of a set of rate equations which we present in Sec. IV C.

Figure 4 compares the temperature dependence of the PL decay time ($1/e$ time) with that of the PL intensity. The decay curves were measured at low laser powers (60 mW) from 4 to 160 K. Above 160 K the decay time drops below the system response time of 20 μs. As pointed out in Sec. I, the simultaneous decrease of both intensity and decay time with increasing temperature is strong evidence of a competing nonradiative process that decreases the radiative efficiency of the Si:Er center. The decay time corresponds to an effective, internal lifetime τ_{eff} of the excited Si:Er center

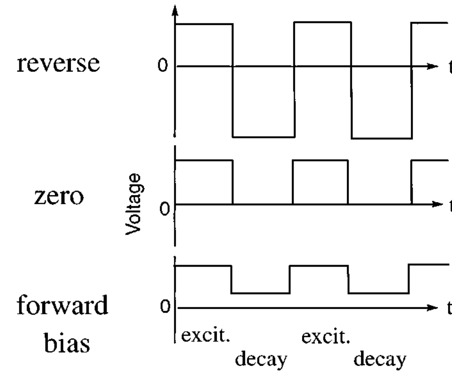

FIG. 5. Pulse scheme for the EL decay experiments.

$$\frac{1}{\tau_{\text{eff}}}=\frac{1}{\tau_{\text{sp}}}+\frac{1}{\tau_{\text{bt}}} \tag{5}$$

reflecting the decay of excited Er centers N_{Er}^{*} by radiative transitions (τ_{sp}) and competing back-transfer processes (τ_{bt}) to the ground state [regime IV in Fig. 1(a)]. When the probability of the nonradiative transitions is greater than the spontaneous emission time, the decay time will decrease, and a higher generation rate is required to achieve the same steady-state population of N_{Er}^{*}. This construct is consistent with the changes of the PL power dependence with temperature. As the PL intensity is proportional to $N_{\text{Er}}^{*}/\tau_{\text{sp}}$ the PL intensity will decrease, or more power is needed to achieve the same PL intensity. In Eq. (4) for the power dependence, this decrease of efficiency with temperature is reflected by the increase of the parameters c_4 or c_5. The physics of the temperature-dependent loss process is contained in the variation of c_4 and c_5 with temperature. The correlation of decay time and emission intensity at $\lambda=1.54$ μm in Er-doped silicon was previously reported in Ref. 14. Back transfer processes at RE in semiconductors have been discussed not only for the Si:Er system,[12,14] but also for InP:Yb,[19–21] InP:Er,[22] GaAs:Er,[23] $\text{InP}_{0.93}$ $\text{As}_{0.07}$:Yb,[24] and GaP:Nd.[25]

The increasing slope of the PL vs power curves and the extrapolation to high powers indicate that for all temperatures the intensity would saturate at the same level if enough power could be provided. This behavior confirms that the total number of optically active Er centers N_{Er} is independent of temperature. Coffa *et al.*[26] recently showed a similar dependence of electroluminescence intensity on drive current.

B. Electroluminescence decay curves

In the section we investigate the processes which decrease the radiative efficiency with increasing pump power and temperature. In order to evaluate the participation of free carriers via an impurity Auger process [Fig. 1(c)] we measured EL decay curves at 40 K, applying different bias conditions during the decay half-cycle [Fig. 5]. Figure 6 shows that under zero-bias conditions the decay signal is composed

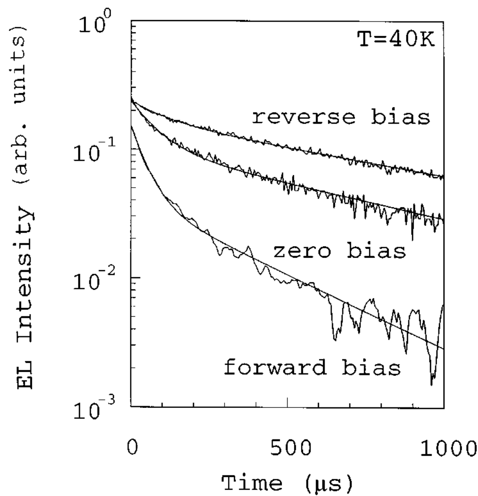

FIG. 6. EL decay at 40 K for different bias conditions during decay cycle (sample *C*).

of fast and slow components. Fitting two exponentials to the measured profiles we obtain $1/e$ decay times of 82 and 770 μs contributing to the signal in an intensity ratio of 1:1. Under reverse bias the contribution of the fast component is strongly decreased, and the two-exponential fit yields 110 μs and 1 ms and with an intensity ratio of 2:5. A small forward bias results in very a fast decay (380 and 49 μs, intensity ratio 1:3). At higher temperatures the effect of reverse bias on the contribution of the long component is even more pronounced. At 100 K (Fig. 7) the two-exponential fit yields 20 μs/700 μs (intensity ratio 8:1) under zero bias, and 33 μs/820 μs (intensity ratio 1:1) under reverse bias.

We observe a related phenomenon when pumping with different drive currents and measuring the EL decay under zero-bias conditions. Figure 8 shows three decay curves for 2, 16, and 70 mA, respectively. At the lower drive current the double-exponential fit yields two components with 199 and 930 μs with an intensity ratio 1:2. Increasing the drive

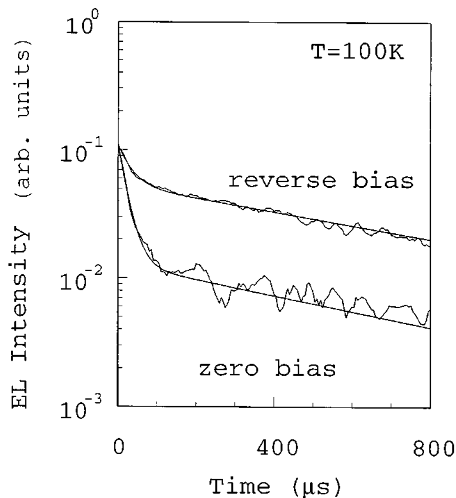

FIG. 7. EL decay at 100 K under reverse and zero-bias conditions (sample *C*).

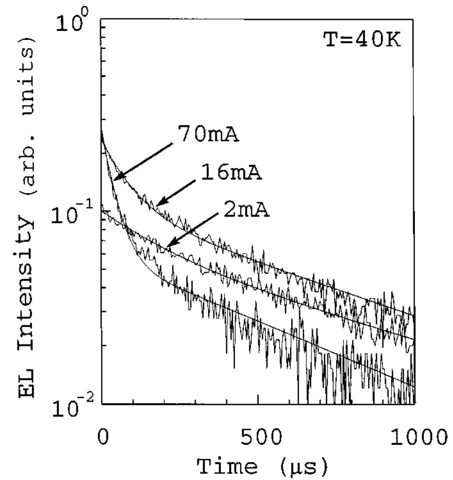

FIG. 8. EL decay at 40 K for different drive currents (sample *C*).

current to 70 mA the intensity ratio of fast (40 μs) to slow (675 μs) components becomes 4:1. To examine these two components we recorded EL spectra at different bias conditions during decay (Fig. 9) and for different drive currents followed by zero bias (Fig. 10) during the decay. The spectra are identical regardless of the different decay profiles.

The EL decay experiments show that the effective lifetime decreases for forward- relative to reverse-bias conditions. The change of bias from forward to reverse corresponds to an increase of the depletion-layer width. Figure 11(a) shows a spreading resistance profile (SRP) of the LED (sample *C*) and the Er distribution obtained by secondary-ion-mass spectrometry (SIMS). The position of the junction (at a depth of 1.6 μm) is controlled by donors introduced by Er/O implantation and annealing. Capacitance-voltage (*C*-*V*) measurements at 40 K give depletion region widths of 0.4 and 1 μm under zero and reverse bias (16 V), respectively. The Er-doped layer, therefore, is mostly depleted under the applied reverse-bias voltage. At the measurement temperature a large fraction of the Er layer is outside the depletion region at zero bias. Taking into account that the doping profile is almost symmetric near the junction, from the SIMS profile we estimate fractions of 46%, 44%, and 10% of Er ions in the *n*-type, depletion, and *p*-type regions, respec-

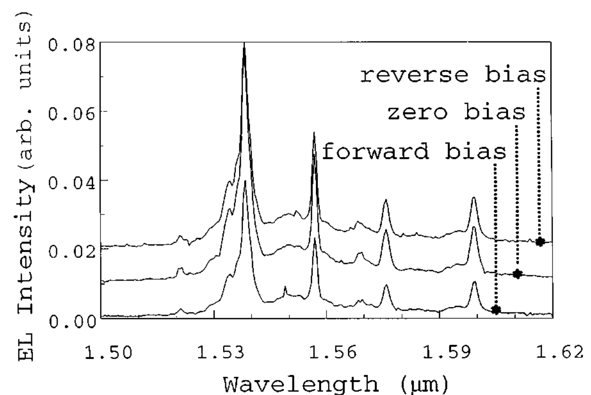

FIG. 9. EL spectra at 40 K for different bias conditions (resolution 8 Å, sample *C*).

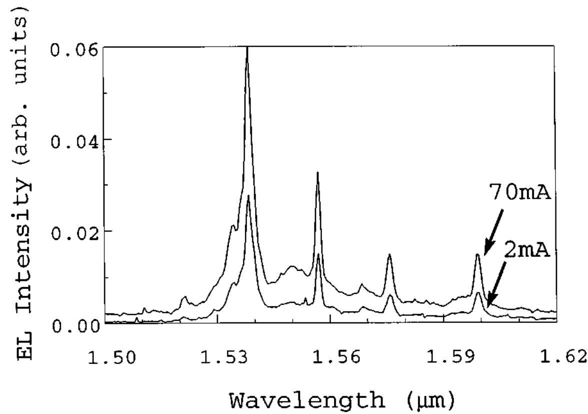

FIG. 10. EL spectra at 40 K for different drive currents at 40 K (resolution 8 Å, sample *C*).

tively, for zero bias. For reverse bias we obtain about 23% (n), 75% (depleted), and 2% (p). Therefore the decrease of decay time at zero bias implies that the probability of the competing nonradiative process [in regime IV of Fig. 1(a)] is

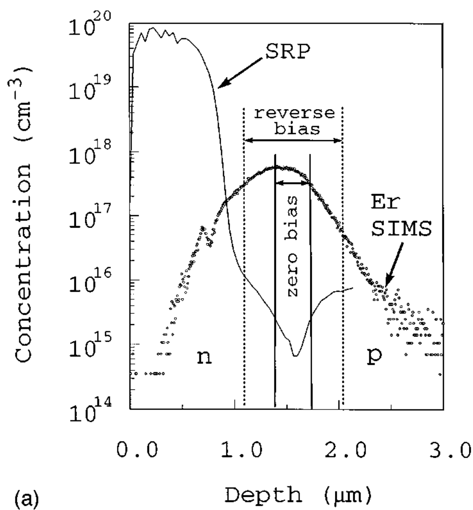

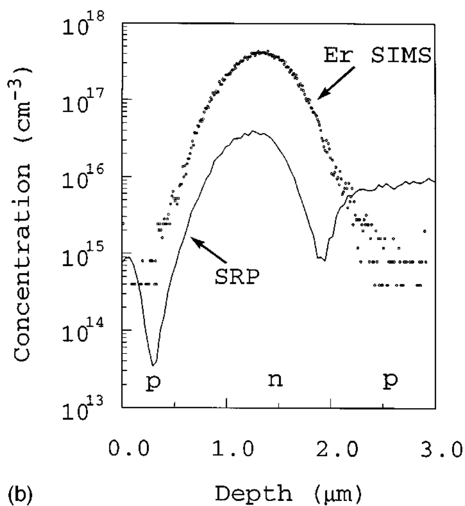

FIG. 11. Spreading resistance and Er-SIMS profiles of (a) sample *C* (LED, deep implanted); (b) sample *A* (Er/O deep implanted and annealed).

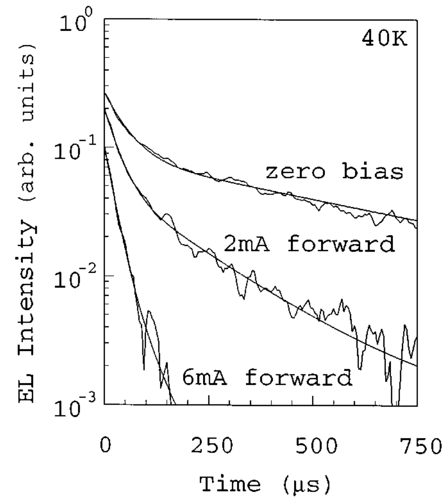

FIG. 12. EL decay curves at 40 K for zero bias and two different forward biases (corresponding to 2- and 6-mA forward current) during decay (sample *C*). A two-exponential fit yields 50 μs/670 μs (intensity ratio 2:1) for zero bias, 33 μs/202 μs (intensity ratio 3:1) for 2 mA, and 23 μs/67 μs (intensity ratio 8:1) for 6-mA.

dependent on the availability of equilibrium free carriers. As shown below (Sec. IV D) the carrier density in the n region is controlled by deep and shallow donors. If the equilibrium free-carrier density increases above 40 K, we expect at higher temperatures a strong short component for zero-bias decay which is confirmed in Fig. 7. The decrease of the zero-bias decay time with increasing temperature and its recovery under reverse bias support the correlation between the probability of the competing nonradiative process and the availability of equilibrium free carriers. The interchange of decay time and equilibrium free carriers is strong evidence of the luminescence quenching by an impurity Auger process. The energy of the excited luminescence center is transferred to free carriers by electron dipole or exchange interaction [Fig. 1(c)]. This process is responsible for effective luminescence quenching at Mn in ZnS,[27,28] as well as Mn, Gd, and Tb in CdF_2.[29,30]

The changes of the decay curves due to different drive currents (Fig. 8) and due to forward bias during the decay (Figs. 8 and 12) indicate that the quenching can also be induced by the injected excess carriers. The contribution of the short decay components increases with injection level. The presence of excess carriers during the decay also leads to an increase of the short contribution, and the decay time of the long component decreases as the forward current during decay is increased (Fig. 12). This result leads to an explanation of the shape of the decay profiles under zero-bias conditions: the excess carrier density decreases rapidly after switching from forward to zero bias. The excess carriers outside the zero-bias depletion region can either recombine or diffuse to the junction, yielding a time-dependent probability of the Auger quenching. The effect of luminescence quenching by excess carriers is particularly evident in Fig. 8: the EL intensity for the highest drive current (70 mA) drops below the EL intensity of the 16- and the 2-mA decay (the intensity scale is identical for all three decay curves). The influence of the excess carrier decay on the EL decay participates in the backtransfer mechanism, which decreases the effective ex-

cited Er lifetime. The analytical fitting by two exponentials is therefore only an approximation which is convenient to describe the convoluted change of the decay curves. Increasing the driving current and, hence, the carrier density in the Er region results in an increase of the fast contribution.

In order to investigate the processes discussed above quantitatively, it is important to consider that the effects on the EL decay curves are due to spatial inhomogeneity, time, and temperature-dependent phenomena. In the next two sections we show how we can separate the impurity Auger effect by excess carriers on one hand, and by equilibrium free carriers on the other hand. PL decay curves at 4 K for different pumping powers and a PL two-beam experiment correlates the back-transfer deexcitation (regime IV) with excess carriers. The results can be simulated with a set of rate equations which couple the excited Er $4f$ shell to excess carriers by the impurity Auger effect. The temperature dependence of PL decay curves at low powers of implanted and annealed samples yield evidence of the back transfer via free equilibrium carriers.

Two decay components with power-dependent ratios of their contribution have also been observed by Coffa *et al.*[14] Their interpretation of two different Er species is not consistent with our investigation, since all centers are excited together, but the relative contributions can be controlled by applying different bias conditions only during the decay. Figure 12 shows that the decay time under forward bias decreases continuously as the forward bias is increased. Therefore the decrease of decay time by increasing drive current or increasing forward bias during decay cannot be ascribed to the saturation of an Er species with a long lifetime. Such saturation would instead result in a change of the intensity ratio of the long and short components, but not in a decrease of the decay time constants of each component. In addition to that, the EL spectra give no evidence of different species, since they are identical for all cases (Fig. 9 for different bias during decay and Fig. 10 for different drive currents). Lombardo *et al.*[31] recently reported on a related EL experiment on metal-insulator-semiconductor structures with amorphous silicon films highly doped with Si and O. By applying a large reverse-bias electroluminescence is obtained which is attributed to impact excitation of Er centers. The observed decrease of decay time for the EL intensity when the pumping level is switched to a lower level was attributed to the continuous pumping only without invoking the possibility of Impurity Auger quenching. It should be noted that despite the similarity between the two experiments, there are large differences in relevant materials properties (excess carrier lifetimes, band structure, etc.), device structure and excitation mechanism. In our devices, no luminescence can be obtained for reverse biases up to 60 V. Whereas the decrease of decay time under small forward bias could be due to continuous pumping only, the differences in decay time which we observe between decay during reverse bias and zero bias can only be explained by a dependence of the excited-state lifetime on the availability of free carriers. As we will show in Sec. IV C by modeling quantitatively a more transparent PL experiment, the strong decrease of decay time for small forward bias and the changes of decay time due to different injection levels support the conclusion that an impurity Auger effect with excess carriers can effectively quench the luminescence of Er in crystalline silicon at low temperatures.

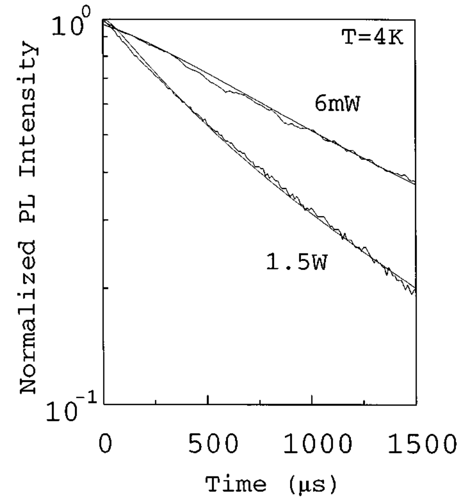

FIG. 13. PL decay curves at 4 K for two different laser powers, solid lines, simulated profiles with rate equations (8a)–(8c).

C. Energy back transfer by the impurity Auger effect via excess carriers

The role of excess carrier impurity Auger back transfer is supported by PL decay curves for two different laser powers at 4 K of implanted and annealed samples (sample A, without additional emitter implant) as shown in Fig. 13. The low temperature and the absence of a collecting junction results in a considerably longer time for the decay of the excess carrier density. The observed initial decay time therefore is much longer ($\sim$200 μs). In order to separate the effect of excess free carriers from equilibrium carrier quenching we performed a two-beam PL experiment at 4 K: a chopped HeNe Laser (8 mW) was used for excitation and a 488-nm Ar-ion laser provided a cw background generation. As shown in Fig. 14 the increase of the cw laser power results in

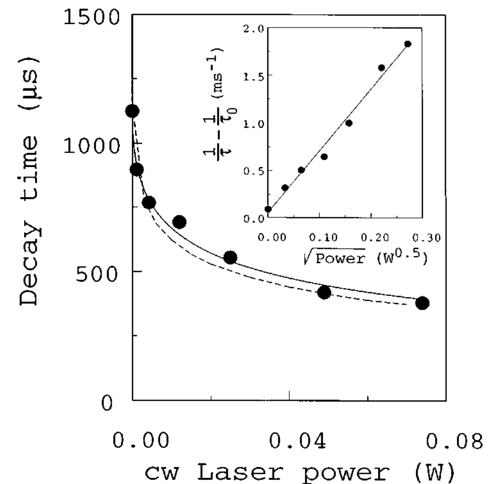

FIG. 14. PL two-beam experiment at 4 K: decay time vs cw laser power; symbols, measured data; the solid line is fitted by Eq. (6); the dashed line is the simulation result (implanted and annealed sample).

a strong decrease in the $1/e$ decay time. This result is analogous to the case of decay during forward bias in Fig. 12.

A similar experiment was performed by Benyattou *et al.*[32] They showed that free-carrier Auger processes decrease the pumping efficiency of Er in GaAs. However, no influence of cw background generation on decay time was observed. Since the excess carrier lifetimes are much shorter in III–V compounds than in Si a considerable photon flux is required to generate an appreciable injection level. The dependence of decay time on cw laser power, i.e., generation rate G, provides, moreover, insight into the excitation process. In the inset of Fig. 14 we replotted the data as $1/\tau_{\rm eff}-1/\tau_0$ vs the square root of the pumping power and obtained a linear relationship. τ_0 is the decay time without secondary illumination. Therefore the relationship between decay time and background carrier generation rate (which is proportional to the power of the second beam) is given by:

$$\tau_{\rm eff}=\frac{\tau_0}{1+c_6\sqrt{G}}, \tag{6}$$

where c_6 expresses the proportionality between $1/\tau_{\rm eff}-1/\tau_0$ and G.

By rewriting Eq. (5) with $\tau_{\rm bt}^{-1}=c_A n$ for an Auger-type process

$$\frac{1}{\tau_{\rm eff}}=\frac{1}{\tau_{\rm sp}}+c_A n, \tag{7}$$

we find that the excess carrier concentration n is proportional to the square root of the generation rate G. This functional dependence implies that the excess carrier concentration is controlled by a bimolecular formation of excitons (as assumed in Sec. IV A). At these low temperatures all recombination processes most likely involve excitons: the indirect band gap of Si inhibits direct band-to-band transitions, and recombination via deep levels is believed to occur via excitonic Auger processes.[33,34] As the Er luminescence is maximal at low temperatures and low excitation levels, we can conclude that excitons are also involved in the Si:Er excitation process, as has been proposed previously.[17]

The following three rate equations, involving the excess carrier density n, the density of excitons N_x, and the concentration of excited Er centers $N_{\rm Er}^*$, can reflect all the features of the excitation and deexcitation processes [see Figs. 1(a)–1(c)]:

$$\frac{dn}{dt}=G-dn^2 \tag{8a}$$

$$\frac{dN_x}{dt}=an^2-c_{A,x}nN_x-\frac{N_x}{\tau_{\rm ex}}\left(1-\frac{N_{\rm Er}^*}{N_{\rm Er}}\right), \tag{8b}$$

$$\frac{dN_{\rm Er}^*}{dt}=\frac{N_x}{\tau_{\rm ex}}\left(1-\frac{N_{\rm Er}^*}{N_{\rm Er}}\right)-N_{\rm Er}^*\left(\frac{1}{\tau_{\rm bt}}+c_{A,{\rm Er}}N_e\right). \tag{8c}$$

Equation (8a) describes the generation of carriers and the formation of excitons. The last term reflects the results of the two-beam experiment. The excess carrier density is controlled by bimolecular formation of excitons. The form of the functional dependence of PL intensity on power [Eq. (4)] indicated that there are two loss mechanisms, the rates of which increase with the excess carrier density. We identified one as the impurity Auger back transfer (regime IV). The second one is most likely the loss of excitons by Auger-type processes [Fig. 1(b)] with free carriers (regime III) which is accounted for by the second term in Eq. (8b). The third term in the exciton equation describes the excitation (τ_e) of the Er (regime III). The factor in parentheses in the last term is the residual fraction of unexcited Er centers ($N_{\rm Er}$ is the total number of Er centers). This value approaches zero at high excitations, leading to a saturation in luminescence intensity. The last equation (8c) for the concentration of excited Er reflects the two possible deexcitation paths (regime IV): radiative emission with spontaneous emission time τ_r and impurity Auger quenching which is proportional to the density of free carriers.

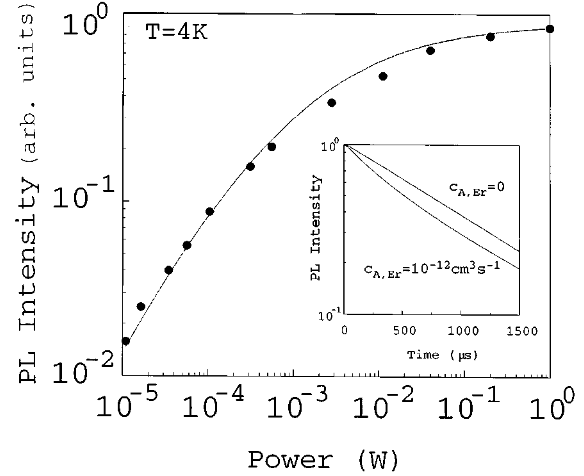

FIG. 15. Simulation results: power dependence at 4 K; data points (symbols) are from the 4 K curve in Fig. 3; the solid line is simulated with $\tau_r=1$ ms, $\tau_e=4$ μs, $a=10^{-12}$ cm^{-3} s^{-1}, $c_{A,x}=1\times10^{-10}$ cm^3 s^{-1}, and $c_{A,{\rm Er}}=10^{-12}$ cm^{-3} s^{-1}. Inset: simulated decay curves for high generation rates ($G=10^{22}$ cm^{-3} s^{-1}) illustrating the effect of impurity Auger back transfer on the decay curve. The intensity is normalized.

Figure 15 demonstrates the good agreement between the simulated and measured power dependence. The fitting function Eq. (4) can be derived from the analytical solution for the steady state in the limit of $N_{\rm Er}^*\ll N_{\rm Er}$ given by

$$I(G)=\frac{N_{\rm Er}^*}{\tau_{\rm sp}}=\frac{G}{\left[1+\frac{\tau_{\rm ex}}{c_{A,x}}\left(\frac{G}{a}\right)^{1/2}\right]\left[1+\frac{\tau_{\rm sp}}{c_{A,{\rm Er}}}\left(\frac{G}{a}\right)^{1/2}\right]}. \tag{9}$$

The good fit with Eq. 4 which is valid for $N_{\rm Er}^*\ll N_{\rm Er}$, seems to indicate that under the present experimental conditions, i.e., Er peak concentration and depth, the maximum light output at low temperatures is limited by the Auger processes and not by the number of excitable Er ions. Due to the complex structure of the real samples (spatial inhomogeneity, recombination at surface and implantation defects, etc.) this model provides only a semiquantitative description.

In the following paragraphs we apply these rate equations to describe the PL decay curves, the power dependence of

the emission intensity and the two-beam experiment and discuss the reasonableness and the consistency of the parameters. Assuming that the maximum applied power (1.6 W in a beam spot of 2-mm diameter) corresponds to a generation rate of 10^{21} cm^{-3} s^{-1}, we obtain the following set of parameters: $\tau_{sp}=1$ ms, $\tau_{ex}=4$ μs, $a=10^{-12}$ cm^3 s^{-1}, $c_{A,x}=1\times10^{-10}$ cm^3 s^{-1}, and $c_{A,\mathrm{Er}}=(0.2\ldots1)\times10^{-12}$ cm^3 s^{-1}. The solid lines in Fig. 13 show the simulated decay profiles for two different excitation powers, demonstrating that the observed fast component indeed appears at high generation rates and is due to the initial decay of excess carrier. The inset of Figure 15 compares simulated normalized decay curves with $c_{A,\mathrm{Er}}=0$ and $c_{A,\mathrm{Er}}=10^{-12}$ cm^{-3} s^{-1}. In the case of $c_{A,\mathrm{Er}}=0$, i.e., no back transfer, there is no influence of the other loss process (regime III) on the decay time, i.e., in this case the excitonic Auger recombination. The dashed line in Figure 14 illustrates the excellent results of the application of the model and the parameters to the PL two-beam experiment. The strong and nonlinear increase of the effective decay rate τ_{eff}^{-1} (Fig. 14 and inset) with increasing background generation cannot be explained by the continuous pumping only without the Impurity Auger quenching of the Er excited state lifetime with excess free carriers.

Hangleiter and Häcker[35] investigated the process of excitonic Auger recombination [Fig. 1(b)] for low carrier concentrations in Si. In their research on electron-hole-electron recombination processes, they considered the effect of electron-hole correlation due to Coulombic interaction, which enhances the probability of Auger processes particularly at low temperatures and low carrier densities. Introducing an electron-hole correlation factor g_{eeh} the rate for Auger recombination is now $R=g_{\mathrm{eeh}},\, c_A\, n^2p$. The correlation factor depends on the carrier concentration and temperature. From Fig. 2 in Ref. 35 one can see a simple relationship $g_{\mathrm{eeh}}=5\times10^{17}$ cm$^3/n$ which complements the experimental and theoretical data of Hangleiter's paper well in the concentration range between 10^{16} and 10^{18} cm^{-3}. With the free-carrier Auger coefficient for high concentrations,[36] $c_A=2\times10^{-31}$ cm^{-6} s^{-1}, this leads to $R=1\times10^{-12}$ cm^{-3} s^{-1} np. In our simple three-particle model (free electrons, excitons, and Er centers) we split the electron-hole-electron interaction into two subsequent steps: exciton formation and exciton-electron Auger recombination [see Fig. 1(b)]. Since the slower process gives the total rate, we can conclude that the values obtained from our simulations ($a=10^{-12}$ cm^3 s^{-1}, $c_{A,x}=1\times10^{-10}$ cm^3 s^{-1}) agree very well with this work. Note that our simulations [Eqs. (8a)–(8c)] and the fitting to the experimental results cover only the low temperature PL (4 K), where all background carriers are frozen and only excess carriers ($n=p$) are considered.

The model assumptions regarding exciton formation and exciton-electron Auger recombination can also be confirmed by measuring the power dependence of the boron bound-exciton line at 1.14 μm. The binding of an exciton at the neutral boron and the subsequent radiative recombination is a competitive process in regime III.

Since the emission intensity is proportional to the number of excitons, we obtain:

$$N_x=\frac{G}{\left[\dfrac{1}{\tau_e}+c_{A,x}\left(\dfrac{G}{a}\right)^{1/2}\right]}, \tag{10}$$

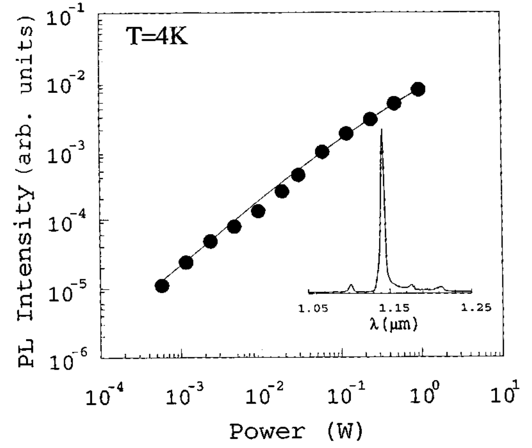

FIG. 16. Power dependence of the boron bound-exciton line intensity (4 K, sample A, PL spectrum in inset). The solid line is fitted with Eq. (11).

$$\mathrm{PL}_{B-\mathrm{BE}}=\frac{c_7p}{c_8+\sqrt{p}}. \tag{11}$$

Figure 16 demonstrates that the intensity of the boron bound-exciton line (see inset) follows this dependence over four decades of excitation laser power.

The coefficient for the impurity Auger effect was calculated by Langer and co-workers.[28,37] Assuming only electric dipole interaction a simple formula was obtained for the impurity Auger coefficient $c_{A,\mathrm{Imp}}$ and the critical density n_0 when radiative and radiationless processes have equal rates:

$$c_{A,\mathrm{Imp}}=(n_0\tau_{sp})^{-1}, \tag{12}$$

$$n_0=4\pi^{5/2}n_r^5\lambda_0^{-7/2}\left(\frac{m^*}{m_0}\frac{\alpha_B}{\alpha_0}\right)^{1/2}. \tag{13}$$

n_1 is the refractive index; λ_0 is the transition wavelength; m^* and m_0 are the effective and free-electron masses, respectively; $\alpha_0=\frac{1}{137}$, and α_B is the Bohr electron radius. Substituting the symbols with the corresponding values for Er in Si ($\lambda_0=1.54$ μm, $\tau_r=1$ ms) we obtain $n_0=7.6\times10^{14}$ cm^{-3}. In agreement with our observations, Langer's theory predicts that impurity Auger processes in silicon become important at relatively low carrier concentrations. The calculated value of $c_{A,\mathrm{Imp}}=1.4\times10^{-12}$ cm^{-3} s^{-1} is in good agreement with our value of $c_{A,\mathrm{Er}}$ obtained above from the application of the rate equations [Eqs. 8(a)–8(c)] to our measured data.

D. Energy back transfer by the impurity Auger effect via equilibrium free carriers

Spreading resistance measurements on Er/O-implanted and -annealed samples revealed the type conversion of a large fraction of the implanted layer from p to n-type [Fig. 11(b), sample A]. The comparison with the SIMS profile shows that most of the implanted Er lies in the n-type region as well as in the depletion region of the second junction. Temperature-dependent Hall-effect measurements on a shallow implanted sample (sample B) show the presence of shallow and deep donors after the implantation and annealing process, with thermal activation energies of 20 and 160

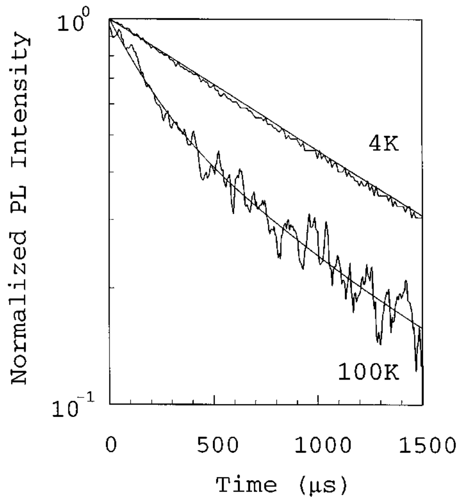

FIG. 17. Low-power PL decay curves and fitted exponentials (60 mW, sample A); 4 K; one exponential (1290 μs); 100 K, two exponentials (270 and 1033 μs).

meV.[38] As the concentration of shallow donors ($\sim 5\times 10^{16}$ cm^{-3}) is about six times higher than the shallow boron acceptors (8×10^{15} cm^{-3}) the apparent activation energy measured for temperatures above 70 K corresponds to the half of the true ionization energy of 40 meV (i.e., negligible compensation). In this section we show that these shallow donor states provide the electrons for the impurity Auger backtransfer process.

Figure 17 shows the PL decay curves at low excitation powers for three different temperatures. At 4 K a single-exponential decay is observed with a time constant resonant of 1290 μs. With increasing temperatures a fast component appears. Here we can rule out the effect of excess carriers discussed in Sec. IV C. There is no fast component at 4 K at these low excitation powers. For a given pumping power the quenching effect via excess carriers should be most pronounced at low temperatures where the excess carrier lifetimes are long enough. Considering the spatial distribution of the Si:Er centers presented in Fig. 1(b), we propose that the two decay components correspond to the decay of Er centers in the n-type ($n>0$) and depletion regions ($n=0$). In the n-type region the concentration of equilibrium free electrons increases with increasing temperatures by ionization of the shallow donor states. These free carriers reduce the effective excited-state lifetime of Si:Er centers in this region by the impurity Auger effect. While the temperature dependence of the contributions, i.e., the ratio of intensities, of the fast and slow components depend on the distribution of generated carriers and the spatial distribution of donors, the decay time should have a simple temperature dependence. Rewriting Eq. (6) with the thermally activated concentration of carriers, we obtain

$$\tau_{\mathrm{eff}}=\left\{\frac{1}{\tau_{\mathrm{sp}}}+c_0\exp\left(-\frac{E_A}{k\cdot T}\right)\right\}^{-1}. \tag{14}$$

In Fig. 18 we plot the short decay time as a function of temperature. The solid line is a fit with Eq. (14). We obtain $\tau_{\mathrm{sp}}=1290$ μs, $c_9=0.067$, and $E_A=24$ meV. The activation energy of 24 meV is in good agreement with the free-carrier activation energy obtained from the Hall-effect measurement. The attribution of short and long components to Er centers in the n-type and depletion regions, respectively, is supported by the EL decay experiments in Sec. IV C where we were able to control the contribution of these components by varying the depletion width through a reverse bias during the decay half-cycle. We showed above that a short decay component arises with an increasing excitation level due to the excess carrier quenching. The relative contribution and the time constants therefore depends on the net carrier concentration given by background doping and process-induced electrically-active defects, and on the spatial homogeneity and injection level.

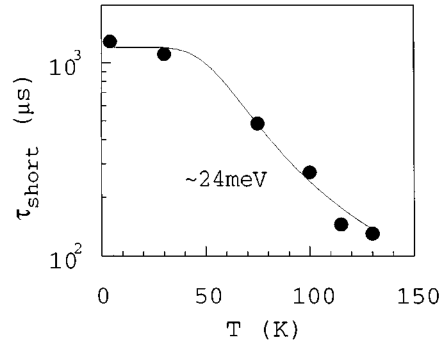

FIG. 18. Temperature dependence of the short PL decay component (60 mW, sample A); the solid line is fitted with Eq. (14).

In order to estimate the upper limit of the contribution of the impurity Auger effect with equilibrium free carriers to the thermal quenching of intensity we replace c_A and n of Eq. (7) with the impurity Auger coefficient obtained from our simulations ($c_{A,\mathrm{Er}}=10^{-12}$ cm^{-3} s^{-1}) and the maximum carrier concentration at 300 K obtained from SRP of sample A (Fig. 16, $n=2\times 10^{16}$ cm^{-3}). We obtain an effective lifetime of 20 μs. Compared to the spontaneous emission time of 1 ms, this would account only for a quenching by a factor of $\tau_{\mathrm{sp}}/\tau_{\mathrm{eff}}=50$ which is much less than observed for low laser powers ($\sim 10^3$). It is evident, however, that the first step of thermal quenching between 4 and 100 K (Fig. 2) can be attributed to impurity Auger back transfer with equilibrium free carriers. The apparent activation energy $E_t=10$ meV for intensity quenching obtained from the fitting by Eq. (2) is different from the value obtained from the initial decay time, because the total emission intensity is determined by Si:Er centers in all three regions (n, p, and depletion layer).

Taguchi, Nakagome, and Takahei[20] consider the impurity Auger effect with bound carriers as a possible quenching mechanism for Yb in InP at low temperatures. If the carriers were bound to the Er with a binding energy of 20 meV, we would, however, expect an increase of lifetime with temperature as the thermalization of these carriers would inhibit this nonradiative relaxation process of the excited $4f$ shell. Taguchi, Nakagome, and Takahei proposed that the Yb luminescence may be quenched by the impurity Auger process through electrons that are captured by the Yb-related trap from distant shallow donors after the excitation process. The temperature behavior of such an indirect process is less obvious: it depends on the ionization energies of the shallow donor and the RE-related trap. We cannot not rule out such a

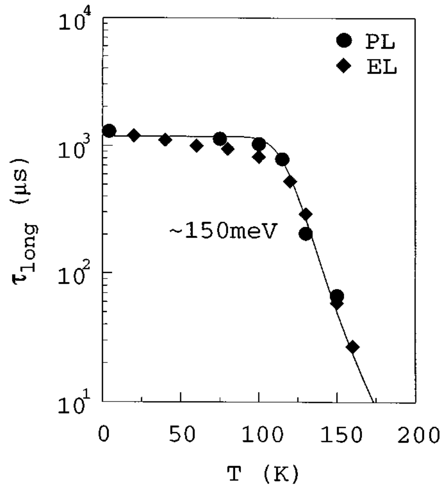

FIG. 19. Temperature dependence of the long component: PL decay of sample *A* at low power (circles) and EL decay under reverse bias (sample *D*). Solid lines are fitted by Eq. (14), yielding an activation energy of 150 meV for both sets of data.

process without further knowledge about the nature of the observed deep and shallow donors in the Si:Er:O system. We believe, however, that the impurity Auger effect with free carriers is more likely the dominant process: first, because all our results, i.e., the quenching by excess carriers, EL decay under reverse bias and the correlation between the temperature dependence of the low-power short component and the free-carrier concentration, can be explained by this process; second, because theoretical predictions and experimental results on CdF_2:Mn (Ref. 29) show that the impurity Auger quenching by bound carriers is about two orders of magnitude smaller than that by free carriers.

The disagreement between the observed quenching rate of the emission intensity and the extrapolated lifetime quenching by the impurity Auger effect suggests that the observed activation energy of 160 meV cannot be due to impurity Auger quenching by free carriers which are released from deep donors at E_c-160 meV. In Sec. IV E we present experimental evidence of this important conclusion. We reveal the presence of a second back-transfer process from Si:Er which is responsible for the thermal quenching above 100 K.

E. Evidence of a second back-transfer process

In Sec. IV D we showed that the fast component in the low-power PL experiment, which arises at higher temperatures, can be attributed to the impurity Auger effect via free equilibrium carriers in the n-type region. In Fig. 19 we plot the temperature dependence of the long component that we attribute to Er centers in the depletion region (circles). Due to the absence of free equilibrium carriers, the decay time is almost constant in the range from 4 to 100 K. For higher temperatures, however, the long component also decreases rapidly. The solid line is a fit with Eq. (14), which yields an activation energy of about 150 meV.

In order to examine the role of the depletion region width we performed a corresponding EL experiment on a processed 400 keV LED (sample D). The EL decay curves were measured under reverse-bias conditions. Fig. 19 (diamonds) demonstrates that the long decay component shows the same dependence as in the PL experiments. Above 100 K the long component decreases rapidly with the same activation energy (150 meV), and it falls below the system response time at temperatures above 160 K. We have shown by the EL experiments (Sec. IV B, Figs. 6 and 7) that the contribution of the long component can be controlled by the reverse bias. The control by reverse bias and the small decrease up to 100 K therefore show indeed that the long decay component of the EL decay under reverse bias is dominated by Si:Er centers inside the depletion region.

By temperature dependent C-V measurements we confirmed that the reverse bias depletion layer capacitance of the shallow implant LED increase only by about 5% from 100 to 300 K. As the capacitance is inverse proportional to the depletion layer width, we can conclude that the depletion width does not change significantly in this temperature range. The narrower distribution of Er for the shallow implant (peak depth at 130 nm) ensures that all Er centers are inside the large reverse-bias depletion region (800 nm). Hence, despite the absence of free carriers we can observe a strong decrease of the excited Er lifetime above 100 K. This result leads to the important conclusion that the thermal quenching above 100 K must be caused by a different, nonradiative energy back transfer mechanism.

The quenching activation energy of 150 meV corresponds approximately to the second activation energy obtained from the temperature dependence of the emission intensity [Fig. 2 and Eq. (2)]. The energy is close to the deep donor level which we obtained from Hall effect. Er/O-related states in the band gap close to E_c-160 meV have been previously found by other groups by deep-level transient spectroscopy measurements.[10,11,39] In Refs. 10 and 11 the authors proposed the thermalization of the exciton bound to a E_c-150 meV band-gap state as the quenching mechanism for the luminescence of Er in Si. This process, however, can only decrease the pumping efficiency (regime III, Fig. 1) and should not result in the decrease of the effective excited state lifetime, as discussed above.

The paper by Coffa *et al.*[14] reported the decrease of the $1/e$ time of the two observed decay components with temperature. This result was attributed to backtransfer processes in agreement with our results. As mentioned above, their interpretation of the components as two Er species cannot account for our decay experiments under different bias conditions. In Ref. 11 the decay curves were decomposed into two decay components with $1/e$ times of $\sim$80 μs and $\sim$1 ms (Figs. 3 and 4 in Ref. 11). The temperature dependence of the time constants is not shown in that paper. It is argued, however, that in impurity-rich Er-doped Si the luminescence intensity is dominated by an Er configuration with a fast decay. The thermal quenching is attributed to the thermalization of the bound exciton. Conversely, the analysis of the preceding sections show that in our Er/O-doped samples both decay components decrease subsequently with increasing temperature below the time resolution of our system (20 μs). Due to this experimental limitation our conclusion on the second back transfer is limited to the temperature range below 200 K. Shin *et al.* recently[40] investigated the Er luminescence of hydrogenated amorphous silicon films. The simultaneous decrease of luminescence intensity was ex-

plained by back-transfer processes, too. Conversely, Van den Hoven *et al.*[41] recently reported on the thermal quenching behavior of amorphous silicon films highly doped with Si and O. Little temperature quenching of intensity was observed, and the decay curves showed two components with temperature independent time constants and ratio of contributions. Little thermal quenching was also observed for ErO_x nanocrystals, a silicon matrix,[42] and Er implanted in porous silicon.[43] The understanding of these interesting noncrystalline silicon-based materials may help to understand the physics of Er in crystalline Si. It should be noted, however, that these materials are distinctively different, and often much less defined in terms of structure, chemistry, and electronic properties, particularly the band gap.

As a possible second backtransfer process we suggest the nonradiative energy transfer from the excited Si:Er to the excitation of a carrier bound to the 160 meV donor level. This transition requires thermal energy to supply the energy difference between the 0.81 eV $4f$ transition energy and the distance between the valence band and donor level $\Delta E=(E_c-0.16\text{ eV})-0.81\text{ eV}=0.15\text{ eV}$. A similar process has was proposed for Yb in InP by Taguchi, Takahei, and Horikoshi.[21]

V. CONCLUSION

We have showed that the thermal quenching of the Er luminescence in Si is caused by nonradiative energy backtransfer processes. The total number of excitable Er remains constant with temperature. We have demonstrated that the impurity Auger process is the dominant quenching mechanism for Er in Si below 100 K. The observed fast initial decay component at high pumping powers was attributed to the decay of the excess carrier concentration which results in a time dependent probability of the nonradiative energy back transfer. Considering exciton formation, exciton-electron Auger recombination and the impurity Auger effect with free (excess) carriers, the power and time dependence can be well described by analytic simulation. We have shown evidence of an additional backtransfer process with an activation energy of about 150 meV which sets in above 100 K.

The involvement of the $4f$ shells makes rare-earth centers unique among other recombination centers in semiconductors. First, excitation and emission occur between discrete energy levels. Since $4f$ electrons are not valence electrons, no phonon replica can be observed in the PL spectra. Second, although the recombination energy of electron-hole pairs or (bound) excitons is not resonant with the $4f$ transition energy, the excitation process is surprisingly efficient at low temperatures, compared to optical pumping of Er in glass hosts or other luminescence mechanisms in silicon. The long spontaneous emission time provides that $\tau_{ex}\ll\tau_{sp}$. Hence, the recombination energy is stored in the $4f$ shell for a time which can be longer than the excess carrier lifetime. This energy storage, however, causes a vulnerability to nonradiative energy backtransfer processes like the impurity Auger process, as we show for the case of Er in Si. The improvement of room-temperature quantum efficiency will require a profound understanding of these backtransfer processes and of the excitation mechanism, too. As it has already been shown experimentally, the ligands, like oxygen or flourine, play a crucial role in the enhancement of light emission from Er in Si.[7–11] Optimization of the role of the ligands in the excitation and back transfer processes, through band-gap states, crystal field engineering or coupling to the lattice, is the pathway to increased quantum efficiency.

ACKNOWLEDGMENTS

We wish to express our gratitude to Shelby Nelson from Colby College, ME, for the Hall-effect measurements. This work was sponsored in part by ARPA/Rome Laboratories, Hanscom/AFOSR under Contract No. F19628-92K-0012 and F19628-95-C-0049. J. P. was supported by the Deutsche Forschungs Gemeinschaft.

[1] H. Ennen, J. Schneider, G. Pomrenke, and A. Axmann, Appl. Phys. Lett. **43**, 943 (1983).

[2] B. Zheng, J. Michel, F. Y. G. Ren, L. C. Kimerling, D. C. Jacobson, and J. M. Poate, Appl. Phys. Lett. **64**, 2842 (1994).

[3] F. Y. G. Ren, J. Michel, Q. Sun-Paduano, B. Zheng, H. Kitagawa, D. C. Jacobson, J. M. Poate, and L. C. Kimerling, in *Rare Earth Doped Semiconductors*, edited by G. S. Pomrenke, P. E. Klein, and H. Langer, MRS Symposia Proceedings No. 301 (Materials Research Society, Pittsburgh, 1993), p. 87.

[4] D. J. Eaglesham, J. Michel, E. A. Fitzgerald, D. C. Jacobson, J. M. Poate, J. L. Benton, A. Polman, Y.-H. Xie, and L. C. Kimerling, Appl. Phys. Lett. **58**, 2797 (1991).

[5] J. S. Custer, A. Polman, and H. M. van Pinxteren, J. Appl. Phys. **75**, 2809 (1994).

[6] A. Polman, J. S. Custer, E. Snoeks, and G. N. van den Hoven, Nucl. Instrum. Methods Phys. Res. Sect. B **80–81**, 653 (1993).

[7] P. Favennec, H. L'Haridon, D. Moutonnet, M. Salvi, and M. Gauneau, Jpn. J. Appl. Phys. **29**, L524 (1990).

[8] F. Y. G. Ren, J. Michel, D. C. Jacobson, J. M. Poate, and L. C. Kimerling, in *Materials Synthesis and Processing Using Ion Beams*, edited by R. J. Colbertson, O. W. Holland, K. S. Jones, and K. Maen, MRS Symposia Proceedings No. 316 (Materials Research Society, Pittsburgh, 1994), p. 493.

[9] J. Michel, J. L. Benton, R. F. Ferrante, D. C. Jacobson, D. J. Eaglesham, E. A. Fitzgerald, Y.-H. Xie, J. M. Poate, and L. C. Kimerling, J. Appl. Phys. **70**, 2672 (1991).

[10] S. Libertino, S. Coffa, G. Franzo, and F. Priolo, J. Appl. Phys. **78**, 3867 (1995).

[11] F. Priolo, G. Franzo, S. Coffa, A. Polman, S. Libertino, R. Barklie, and D. Carey, J. Appl. Phys. **78**, 3874 (1995).

[12] J. Michel, F. Y. Ren, B. Zheng, D. C. Jacobson, J. M. Poate, and L. C. Kimerling, Mater. Sci. Forum **143–147**, 707 (1994).

[13] S. Coffa, F. Priolo, G. Franzo, V. Bellani, A. Carnera, and C. Spinella, Phys. Rev. B **48**, 11 782 (1993).

[14] S. Coffa, G. Franzo, F. Priolo, A. Polman, and R. Serna, Phys. Rev. B **49**, 16 313 (1994).

[15] Brief preliminary reports on some of the data presented here were given at the *10th Feofilov Symposium on Spectroscopy of Crys-*

tals Activated by Rare Earth and Transition Metal Ions, St. Petersburg, 1995 [SPIE Proc. **2706**, 31 (1995)].

[16]The involvement of electron-hole pairs in the excitation process when a laser is used as the pumping source was shown for instance in Ref. 9 by illumination of an Er/Q-doped sample from the backside. In the following we will, however, comply with the conventional definition of photoluminescence and electroluminescence as luminescence originated by external optical pumping, i.e., laser, and electrical pumping, i.e., e-h pair injection through a pn junction, respectively.

[17]I. N. Yassievich and L. C. Kimerling, Semicond. Sci. Technol. **7**, 1 (1993).

[18]W. J. Miniscalco, J. Lightwave Technol. **9**, 234 (1991).

[19]K. Thonke, K. Pressel, G. Bohnert, A. Stapor, J. Weber, M. Moser, A. Molassiotti, A. Hangleiter, and F. Ascholz, Semicond. Sci. Technol. **5**, 1124 (1990).

[20]A. Taguchi, H. Nakagome, and K. Takahei, J. Appl. Phys. **70**, 5604 (1991).

[21]A. Taguchi, K. Takahei, and Y. Horikoshi, J. Appl. Phys. **76**, 7288 (1994).

[22]X. Z. Wang, A. J. Neuhalfen, and B. W. Wessels, Appl. Phys. Lett. **64**, 466 (1994).

[23]A. Taguchi and K. Takahei, Mater. Sci. Forum **196–201**, 2594 (1995).

[24]A. Kozanecki, K. Karpinska, and Z. Kalisnski, Appl. Phys. Lett. **62**, 85 (1993).

[25]M. Taniguchi and K. Takahei, J. Appl. Phys. Lett. **73**, 943 (1993).

[26]S. Coffa, F. Priolo, G. Franzo, A. Polman, S. Libertino, M. Saggio, and A. Carnera, Nucl. Instrum. Methods Phys. Res. Sect. B **106**, 386 (1995).

[27]N. T. Gordon and J. W. Allen, Solid State Commun. **37**, 1441 (1981).

[28]J. M. Langer, A. Lemanska-Bajorek, A. Suchocki, W. Walukiewicz, and B. Wiktor, J. Lumin. **24-25**, 889 (1981).

[29]A. Suchocki and J. M. Langer, Phys. Rev. B **39**, 7905 (1989).

[30]J. M. Langer, in *Electroluminescence*, edited by S. Shionoya and H. Kobayashi, Springer Proceedings in Physics, Vol. 38 (Springer-Verlag, Berlin, 1989), pp. 16–23.

[31]S. Lombardo, S. U. Campisano, G. N. van den Hoven, and A. Polman, J. Appl. Phys. **77**, 6504 (1995).

[32]T. Benyattou, D. Seghier, G. Guillot, R. Moncorge, P. Galtier, and M. N. Charasse, Appl. Phys. Lett. **58**, 2132 (1991).

[33]A. Hangleiter, Phys. Rev. B **35**, 9149 (1987).

[34]A. Hangleiter, Phys. Rev. B **37**, 2594 (1988).

[35]A. Hangleiter and R. Häcker, Phys. Rev. Lett. **65**, 215 (1990).

[36]D. B. Laks, G. F. Neumark, A. Hangleiter, and S. T. Pantelides, Phys. Rev. Lett. **61**, 1229 (1988).

[37]J. M. Langer, J. Lumin. **40&41**, 589 (1988).

[38]S. Nelson and J. Palm (unpublished).

[39]J. L. Benton, J. Michel, L. C. Kimerling, D. C. Jacobson, Y.-H. Xie, D. J. Eaglesham, E. A. Fitzgerald, and J. M. Poate, J. Appl. Phys. **70**, 2667 (1991).

[40]J. H. Shin, R. Serna, G. N. van den Hoven, A. Polman, W. G. J. H. M. van Sark, and A. M. Vredenberg, Appl. Phys. Lett. **68**, 46 (1996).

[41]G. N. van den Hoven, J. H. Shin, A. Polman, S. Lombardo, and S. U. Campisano, J. Appl. Phys. **78**, 2642 (1995).

[42]A. Thilderquist, J. Michel, S.-T. Ngiam, L. C. Kimerling, and K. D. Kohlenbrander, in *Surface Interface and Stress Effects in Electronic Material Nanostructures*, edited by S. M. Prokes, K. L. Wang, R. C. Cammarata, and A. Christov, MRS Symposia Proceedings No. 405 (Materials Research Society, Pittsburgh, 1996).

[43]A. Namavar, F. Lu, C. H. Perry, A. Cremins, N. Kalkhoovan, and R. A. Soref, J. Electron. Mater. **25**, 43 (1996).